ES Energy & Environment
DOI: https://dx.doi.org/10.30919/esee1097

Engineering Bimetallic Ni-Cu Nanoparticles Confined in MOF-Derived Nanocomposite for Efficient Dry Reforming of Methane

Zichen Du,[1] Fan Chen,[2] Siyuan Fang,[3] Xiaokun Yang,[4] Yulu Ge,[4] Kobi Shurtz,[1] Hong-Cai Zhou,[2] Yun Hang Hu[3] and Ying Li[1,*]

Abstract

To harness the potential of two significant greenhouse gases, CO_2 and CH_4, the dry reforming of methane (DRM) shows promise while generation of syngas (CO and H_2). Ni-based catalysts have shown promising catalytic activities, but they experience significant deactivation due to coke deposition and metal aggregation. In this study, we employed a metal-organic framework (MOF)-templated synthesis of novel structured catalysts, *i.e.* bimetallic Ni-Cu nanoparticles confined in MOF-derived carbon/ZrO_2 nanocomposite (NiCu/C/$ZrO_{2(MD)}$). Alloying a small amount of Cu with Ni reduced the overall metal particle size, enhanced CO_2 adsorption and conversion, and facilitated NiO reducibility to Ni. In addition, the catalyst offered nanoconfinement of Ni-Cu NPs by the MOF-derived C/tegragonal-ZrO_2 framework, which provided a large surface area, featured strong metal-support interaction, and hindered the detrimental filamentous carbon deposition and metal aggregation during DRM process. As a result, the 9Ni1Cu/C/$ZrO_{2(MD)}$ catalyst with a Ni/Cu weight ratio of 9:1 delivered high and stable DRM activities over 100-h DRM, with average CO_2 and CH_4 conversions at 76% and 77%, respectively, and H_2/CO molar ratio at 1.07. This DRM performance is among the top ones reported in the literature, and it is much higher than that of a ZrO_2-supported bimetallic Ni-Cu catalyst prepared by direct calcination with the same Ni/Cu weight ratio, 9Ni1Cu/$ZrO_{2(DC)}$. This work demonstrates the importance of two advanced DRM catalyst structures, bimetallic NiCu alloying and nanoconfinement in porous catalytic carbon/ZrO_2 support, the combination of which significantly promoted carbon management and enhanced DRM activities.

Keywords: Dry reforming of methane; Bimetallic catalyst; Nanocomposite; Greenhouse gas control; Thermocatalysis.
Received: 09 January 2024; Revised: 05 February 2024; Accepted: 12 February 2024.
Article type: Research article.

1. Introduction

Dry reforming of methane (DRM) is a promising and attractive technique that converts two major greenhouse gases (CO_2 and CH_4) into syngas (H_2 and CO).[1,2] However, activation of C-H bonds in CH_4 and C-O bonds in CO_2 require a high energy input. Therefore, the advancement of efficient catalysts is critical to achieve an efficient DRM process.[3] Noble metal catalysts, such as Pt, Pd, Rh, and Ru, were reported to possess efficient DRM catalytic activities,[4-7] but the high cost and low availability restrict their large-scale commercial applications. Extensive studies have been conducted on transition metals, particularly Ni, a promising alternative due to their relative earth abundance and high initial catalytic activities.[8-10]

However, coke formation on Ni-based catalysts due to CH_4 decomposition and CO disproportionation, as well as sintering of Ni at high temperatures, poses a challenge to achieve efficient and stable DRM activities for commercial use.[11-13] One popular strategy to overcome these issues is the design of bimetallic Ni-based systems.[14,15] The combination of two metals in a bimetallic phase can lead to increased DRM performance compared to that of the monometallic phase due to fine-tuned electronic and geometric effects. For instance, the coexistence of two metals in the catalyst might lead to a decrease of overall metal particle size and a decrease in coke formation, especially when a noble metal, such as Pt, Pd, or Rh, is present.[16,17] An alternative to these noble metals is the use of inexpensive and relatively earth-abundant Cu, which possesses a crystal structure akin to Ni, characterized by face-centered cubic metals with comparable lattice constants. With optimized Cu addition, the Ni-Cu alloy size can be

[1] *J. Mike Walker '66 Department of Mechanical Engineering, Texas A&M University, College Station, Texas 77843, United States.*
[2] *Department of Chemistry, Texas A&M University, College Station, Texas 77843, United States.*
[3] *Department of Materials Science and Engineering, Michigan Technological University, Houghton, Michigan 49931, United States.*
[4] *Chemistry Division, Los Alamos National Laboratory, Los Alamos, New Mexico 87545, United States.*
**Email:* yingli@tamu.edu (Y. Li)

minimized.[18] Additionally, CO_2 activation was found to be easier on Ni-Cu than on Ni alone, and the formation of O atoms can be promoted to oxidize CH_x to CO and H_2. These properties allow Ni-Cu based catalysts to display much better DRM performance than Ni-based catalysts. However, excessive amounts of Cu will cover the surface of Ni atoms, reducing CH_4 activation sites, and leading to coke formation thus unstable DRM activities.[19] In addition, migration of Cu atoms towards the exterior and migration of Ni atoms towards the interior on Ni-Cu nanoparticles at high-temperature environment was observed in a molecular dynamics study, which led to a remarkable surface aggregation of Cu atoms and DRM activity loss.[20] To sum up, challenges still exist for Ni-Cu alloy catalysts due to inhomogeneous distribution on the supports, leading to aggregation of Ni-rich and/or Cu-rich alloy particles, which restricted their catalytic activities and long-term stabilities.[15]

Nanoconfinement has been investigated as an effective approach to protect the active metal sites. For example, Shi *et al*. ground the Ni precursors with SBA-15 containing templates, subsequently subjecting them to calcination. This process resulted in a superior dispersion of Ni species within the nano-confined space between the silica wall and template.[21] As a result, a max CO_2 and CH_4 conversion of 64.2% and 53.7% at 750 °C was obtained. Other researchers also applied either nanoconfinement or encapsulating effects on Ni NPs with mainly metal oxide nanostructures/shell. Xu *et al*. observed that employing a seed-directed synthesis method resulted in the Ni@SiO_2-silicalite-1 catalyst, showing complete encapsulation of Ni.[22] This catalyst achieved a performance of CO_2 and CH_4 of ~80% and ~73%, respectively, along with enhanced carbon resistance. Jin *et al*. reported that ZrO_2 overcoating by atomic layer deposition on Ni/Al_2O_3 led to improved metal-oxide interaction and increased oxygen sites at the Ni-ZrO_x interface.[23] Consequently, this catalyst received stable and good DRM performance of 77.2% CH_4 conversion at 700 °C. Qu *et al*. developed a sandwich-structured Ni/kaolinite catalysts with Ni particles tightly packed between layers of kaolinite.[24] Additionally, the carbon deposits served as a pillar agent, enhancing the activity and stability of the catalyst. As a result, the catalyst received an average conversion of around 65% for both CO_2 and CH_4. However, it is noteworthy that these studies solely utilized monometallic catalysts, and the potential advantages stemming from bimetallic effect have yet to be thoroughly explored.

Metal-organic framework (MOF), a new class of crystalline porous material composed of metal cation nodes and organic linkers, has attracted significant research interest for heterogeneous catalysis application.[25] MOF offers benefits, such as elevated surface area, porosity, and the adaptability of functional components at the interfaces and within the porous structure.[26,27] The carbonization of MOF's organic ligands can result in a catalyst that promotes enhanced dispersion of the metal/metal oxide nanocrystallites throughout the carbon framework and prevention of metal/metal oxides from aggregation.[28,29] Additionally, coke formation caused by fast CH_4 decomposition can be suppressed since the MOF-derived framework can act as a barrier to reduce the diffusion rate of CH_4 to the core metal.[30] Liang *et al*. synthesized NiCo-MOF using H_2BDC-NH_2 as the organic link and derived the NiCo@C nanocomposites supported on additional Al_2O_3 catalyst.[31] By conducting DRM at 700 °C on the optimal NiCo@C/Al_2O_3 catalyst for 8 h, the CH_4 conversion decreased from 52 to 43% in the first 2 h and kept at around (42-44) % during the rest 6h, while CO_2 gradually decreased from 76 to 57% during the 8h. The instability was attributable to the metal sintering and coke deposition. Another example of MOF is UiO-66-NH_2, which is constituted by $Zr_6O_4(OH)_4$ nodes characterized by six Zr^{4+} ions arranged in octahedral geometry. Additionally, each octahedral facet incorporates four oxygen atoms or hydroxyl groups at their centers.[32] The surface area of UiO-66-NH_2 ranges from 800 to 1200 m^2/g, which is promising for dispersing metal particles. The porous MOF can also confine metals and minimize growth and agglomeration of these metal particles in high-temperature environments. Furthermore, at high temperatures, UiO-66-NH_2 decomposes into a mixture of C and ZrO_2, which displays strong metal-support interaction and high dispersion of the metal NPs.[33,34] A recent study by Wang *et al*.[35] showed that carbon could be a reaction intermediate and enhance the product yield, which is against the general wisdom that carbon is poisonous to the DRM reaction. Previous studies also showed that ZrO_2 was a thermally stable support and CO_2 dissociation active sites.[36] Therefore, the MOF-derived C/ZrO_2 nanostructure can be a suitable candidate for stable and high-performing DRM.

Based on the above hypothesis, we designed the bimetallic Ni-Cu nanoconfined by MOF-derived nanocomposites as catalysts for DRM. The alloying of Cu with Ni can reduce metal particle size, promote CO_2 adsorption and conversion, and increase Ni reducibility, thus leading to coke resistance and enhanced DRM performance. Additionally, MOF can derive into a C/ZrO_2 nanocomposite in the high-temperature DRM environment, providing enhanced bimetallic dispersion, reactant diffusion and coke resistance. Additional investigations were performed on optimization of bimetallic NiCu compositions, control experiment on NiCu supported on ZrO_2 catalyst, further calcination and pyrolysis of as-prepared NiCu/C/$ZrO_{2(MD)}$ to identify compositional role and nanoconfinement effect of MOF-derived C/ZrO_2 nanostructures.

2. Experimental section

2.1 Catalyst synthesis

The MOF material, UiO-66-NH_2 was synthesized by a solvothermal method.[37] Firstly, 10 mL of N, N-dimethylformamide (DMF, Fisher Scientific) was used to dissolve 0.16g of Zirconium (IV) chloride ($ZrCl_4$, Sigma Aldrich). 250 mg of 2-Aminoterephthalic acid (Sigma Aldrich) was dissolved in 20 ml of DMF. These two solutions were ultrasonicated for 2 min and mixed. Then, to the mixture solutions, 2 ml of concentrated HCl was introduced, followed by ultrasonication for an additional 2 min. Subsequently, the product was placed in an oven at 120 °C overnight. The resulting precipitate underwent centrifugation at 6000 rpm

after cooling down to room temperature and was thoroughly washed DMF and methanol, twice for each. MOF was the product from previous steps, which was then dried at temperature of 70 °C overnight. For comparison purposes, ZrO_2 was alternatively prepared by directly calcinating the same precursor, $ZrCl_4$ directly at 600 °C for 1 h.

Incorporation of Ni, Cu, or Ni-Cu bimetallic nanoparticles was done using the conventional wet impregnation method with aqueous solution of $Ni(NO_3)_2$ and $Cu(NO_3)_2$ (Alfa Aesar, Germany) and a total of 10 wt.% concentration of Ni-Cu was obtained. The ratio of Ni to Cu was tuned by adjusting the $Ni(NO_3)_2$ and $Cu(NO_3)_2$ amounts, and the catalysts are named based on the weight ratio of Ni to Cu, e.g. the catalyst with 9 wt% Ni and 1 wt% Cu incorporated in MOF-derived nanocomposite is named 9Ni1Cu/C/$ZrO_{2(MD)}$, while the catalyst supported on direct-calcinated prepared ZrO_2 is named 9Ni1Cu/$ZrO_{2(DC)}$. After drying overnight at room temperature, the impregnated catalysts were calcinated in an electric furnace at 150 °C, for 3 h to obtain the pristine catalysts. The catalysts are then pre-treated with H_2 at 700 °C to ensure the transition to metal oxides and carbon, described in the following sections.

2.2 Catalyst characterization

Analytical techniques were employed to scrutinize the morphology, structure, and composition of the catalysts. The characterization process included the utilization of Transmission Electron Microscopy (TEM, FEI Tecnai G2 F20ST), X-ray Diffraction (XRD, BRIKER D8), Brunauer–Emmett–Teller (BET) surface area analysis (Micromeritics ASAP 2420 physisorption analyzer), and X-ray Photoelectron Spectroscopy (XPS, Omicron). Following the reduction of the catalysts using H_2/Ar mixture at 700 °C for 2 hours, subsequent characterizations involving TEM, XRD, BET, and XPS were carried out. 0.15 g of fresh catalysts were analyzed using H_2 Temperature-Programmed Reduction (H2-TPR, Micromeritics, AutoChem II 2920) under a mixed 10% H_2/90% Ar flow of 40 sccm, with the temperature ranging from 25 to 700 °C, and a heating rate of 10 °C/min. In addition, 20 mg of spent catalysts were characterized by thermogravimetric Analysis (METTLER TOLEDO, TGA) under an air flow of 40 sccm, with the temperature ranging from 25 to 800 °C, and a heating rate of 10 °C/min and held at 800 °C for 3 hours.

2.3 DRM performance measurements

DRM catalytic activities were assessed using an on-line gas chromatograph (GC 2010, Shimadzu), as used in our previous studies.[36,38,39] Heat was provided by a tube furnace to achieve required temperatures. Real-time feedback to the heating program was achieved with a thermocouple linked to the catalyst surface. For each test, 5 mg of the prepared catalyst was dispersed in 5 ml of deionized water and sonicated to form a uniform ink. Then, the ink was deposited onto a piece of Whatman™ Quartz filter paper and positioned on a catalyst holder, transferred into the tube reactor. For the reaction, the reactor underwent an initial purge with Ar for 30 min at room temperature to eliminate impurities. Catalyst reduction was done with a mixed flow of 23 sccm H_2/28 sccm Ar for 1 hour at 700 °C. Subsequently, the reactor was purged again to eliminate impurities. This high-temperature pre-treatment ensures the conversion of precursors towards metal oxides or carbon.[23] Following this, reactant gases in one channel (10% CO_2/10% CH_4/80% Ar) was set to be 8 sccm and passed through the catalyst surface. During the reaction, the products were only measured to be CO and H_2.

Conversions of CO_2 and CH_4 were calculated as below:

$$Conversion\,\% = \frac{[X]_{in} - [X]_{out}}{[X]_{in}} \times 100$$

In the formula, $[X]_{in}$ and $[X]_{out}$ shows concentrations of CO_2 and CH_4 at the inlet and outlet, respectively. Diving the H_2 concentration to the CO concentration at the outlet gave the H_2/CO ratio.

3. Results and discussion

3.1. Catalyst characterization

Figure 1 and Fig. S1 showed the X-ray diffraction (XRD) patterns of reduced catalysts. MOF-derived carbon/ZrO_2 (C/$ZrO_{2(MD)}$) and direct-calcinated prepared ZrO_2 ($ZrO_{2(DC)}$) were also characterized as references. For all C/$ZrO_{2(MD)}$-based catalysts, diffraction peaks at 2θ = 30.3°, 50.4° and 60.2° of tetragonal crystal ZrO_2 (t-ZrO_2, JCPDS75-9648) and one weak peak at 2θ = 35.2° of monoclinic crystal ZrO_2 (m-ZrO_2) were detected, which agrees with the literature that the pyrolysis process removes the organic ligands of UiO-66-NH_2 yields ZrO_2.[33] For $ZrO_{2(DC)}$-based catalysts, multiple diffraction peaks of m-ZrO_2 and t-ZrO_2, mainly including two characteristic peaks at 2θ = 28.2° and 31.5° of m-ZrO_2, were identified, indicating the dominating species of m-ZrO_2. t-ZrO_2 was generally researched to be more active than m-ZrO_2 for methane conversion process. For instance, Campa *et al*. observed that t-ZrO_2 has a more robust metal-support interaction than m-ZrO_2 due to the greater covalent nature of the Zr-O bond and the presence of more oxygen defects in m-ZrO_2. Consequently, a catalyst supported on t-ZrO_2 demonstrates higher activity in partial methane oxidation compared to one supported on m-ZrO_2.[40] Furthermore, Zhang *et al*. also observed a stronger Ni-ZrO_2 interaction on t-ZrO_2 supported Ni catalyst than m-ZrO_2 thus leading to a higher initial CH_4 decomposition rate and enhanced carbon tolerance during DRM process.[41] In this study, after loading with Ni or NiCu, the t-ZrO_2 peak at 2θ = 30.3° became sharper, indicating a better crystallinity of t-ZrO_2, which is likely due to the oxygen being introduced during the wet impregnation process. On MOF, the wide peak between 20° to 25° can be identified as the amorphous carbon, while such a peak disappeared after Ni or NiCu was loaded, indicating that the amorphous carbon peak was possibly overshadowed by the sharp t-ZrO_2 peak.

In addition, on 10Ni/C/$ZrO_{2(MD)}$, three peaks at 2θ = 44.3°, 51.9°, and 76.4° were identified to be Ni phase (JCPDS 04-0850) while NiO phase (JCPDS 89-3080, at 2θ = 24.7°, 26.6° and 34.9°) was absent, indicating that Ni was fully reduced after the reducing process. On the other hand, on both 9Ni1Cu/C/$ZrO_{2(MD)}$, CuO (JCPDS 41-0254, at 2θ = 38.4°) was not detected. Cu (JCPDS 03-1005, at 2θ = 43.4°, 50.4°) phases were likely to overlap with ZrO_2 peaks, while Ni diffraction peaks became broader and the location of them shifted to

lower angles. Due to the larger atomic radius of Cu (0.128 nm) compared to Ni (0.124 nm), substituting Ni with Cu leads to the expansion of lattice fringes, causing a leftward shift (on 10Ni/C/$ZrO_{2(MD)}$ ~44.3°, on 9Ni1Cu/C/$ZrO_{2(MD)}$, ~43.8°),[42] which evidences the formation of NiCu alloys with a strong interaction instead of a simple mixture of two types of single metal particles.[43] Moreover, no Ni_3C phases (JCPDS 06-0697, at 2θ = 39.3°, 41.7°, 44.7°, and 58.6°) were observed on the samples.[44,45] Additionally, all the metal peaks are sharper and have higher intensities on C/$ZrO_{2(MD)}$-based catalysts compared to $ZrO_{2(DC)}$-based catalysts, especially peak at 2θ = 44.3°, which indicates higher crystallinity of the metals in C/$ZrO_{2(MD)}$-based catalysts. The lower crystallinity on $ZrO_{2(DC)}$-based catalyst might be due to the low temperature of wet impregnation process, while Ni crystallization can be intensified because the strong interaction between metal and carbon derived from MOF will result in higher electron densities thus leading to metal cluster formation.[46,47]

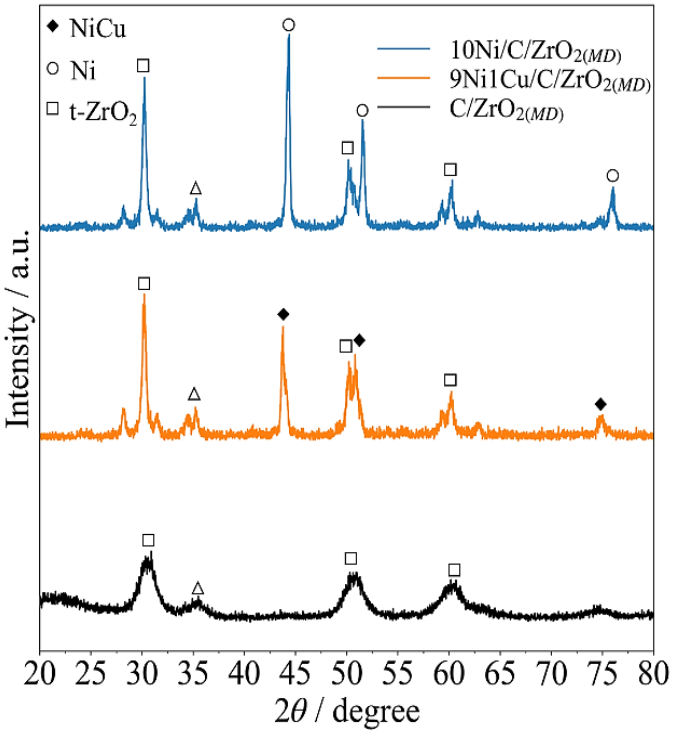

Fig. 1 XRD patterns of C/$ZrO_{2(MD)}$-based catalysts.

The active state of the catalyst is determined by its reducibility. Therefore, the fully oxidized catalysts prepared initially were subjected to analysis through H_2 temperature-programmed reduction (H_2-TPR) (Fig. 2). C/$ZrO_{2(MD)}$ was measured as a reference and no peaks were detected. Two peaks at 237.5°C and 340.7 °C existed on 10Ni/C/$ZrO_{2(MD)}$, and the previous one represents weak, while the later one represents strong, interaction with the supports.[19] With the introduction of Cu, only one peak located at a temperature 311.0 °C on 9Ni1Cu/C/$ZrO_{2(MD)}$ was observed. Since CuO was generally observed to possess a lower reduction temperature than NiO,[48] the only peak can be ascribed to the Ni-Cu alloy, evidenced by the XRD results above. It has also been widely demonstrated that presence of Cu will improve the Ni reducibility, thus maintain the Ni^0 active sites for methane dissociation,[49,50] steam reforming[51] and DRM processes.[52]

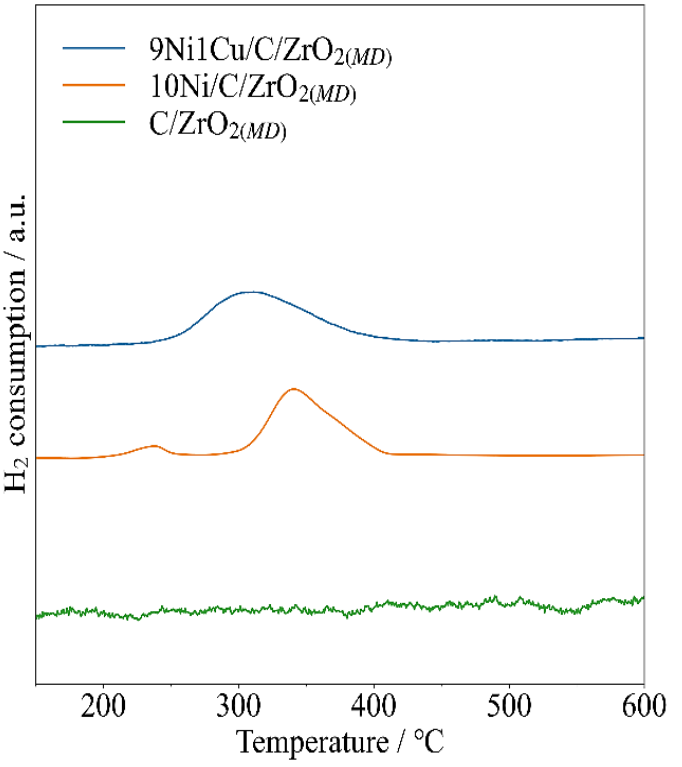

Fig. 2 H_2-TPR profiles of Ni-Cu/C/$ZrO_{2(MD)}$.

Reduced catalysts were further characterized by transmission electron microscopy (TEM) so the morphology can be observed. As in Figs. 3a and 3b, C/$ZrO_{2(MD)}$ displayed a cube morphology, with an average size of 50~60 nm. After loading with 9Ni1Cu, uniformly distributed NiCu nanoparticles were observed within the MOF structure (Fig. 3c). It is also noted that there is no obvious outer shape change, indicating that majority of the NiCu nanoparticles (NPs) were confined inside instead of on the surface of the MOFs.[53,54] On the contrary, the NiCu were mainly aggregated on the surface of the $ZrO_{2(DC)}$ (Fig. S3). The confinement of NiCu nanoparticles by a hybrid C/t-ZrO_2 was further revealed by high-resolution TEM (HRTEM, Fig. 3d). Specifically, C and t-ZrO_2 were found surrounding the NiCu nanoparticles, with a lattice spacing of 0.33 nm and 0.30 nm, corresponding to C (002) plane[55] and t-ZrO_2 (011) plane,[56] respectively. NiCu alloys with the (111) lattice plane was also confirmed with a lattice fringe of 0.20 nm,[57] agreeing with the XRD results. NiCu particles were counted using ImageJ and the particle distribution was presented in Fig. 3e. Average NiCu particle size was 10.1 nm, much smaller than 10Ni/C/$ZrO_{2(MD)}$ (17.6 nm), 10Ni/$ZrO_{2(DC)}$ (19.8 nm) and 9Ni1Cu/$ZrO_{2(DC)}$ (16.5 nm, Figs. S2, S3). Since these catalysts were characterized after reduction at 700 °C, the smaller particle size after Cu addition indicated that the formation of Ni-Cu alloy enhances the stability of crystallites and reduces agglomeration during high-temperature reduction process. A similar finding was reported by Chatla and coworkers[52] where bimetallic catalysts Ni_8Cu_1/Al_2O_3 and $Ni_{10}Cu_1/Al_2O_3$ had a smaller metal particle size than monometallic Ni/Al_2O_3 and led to significant

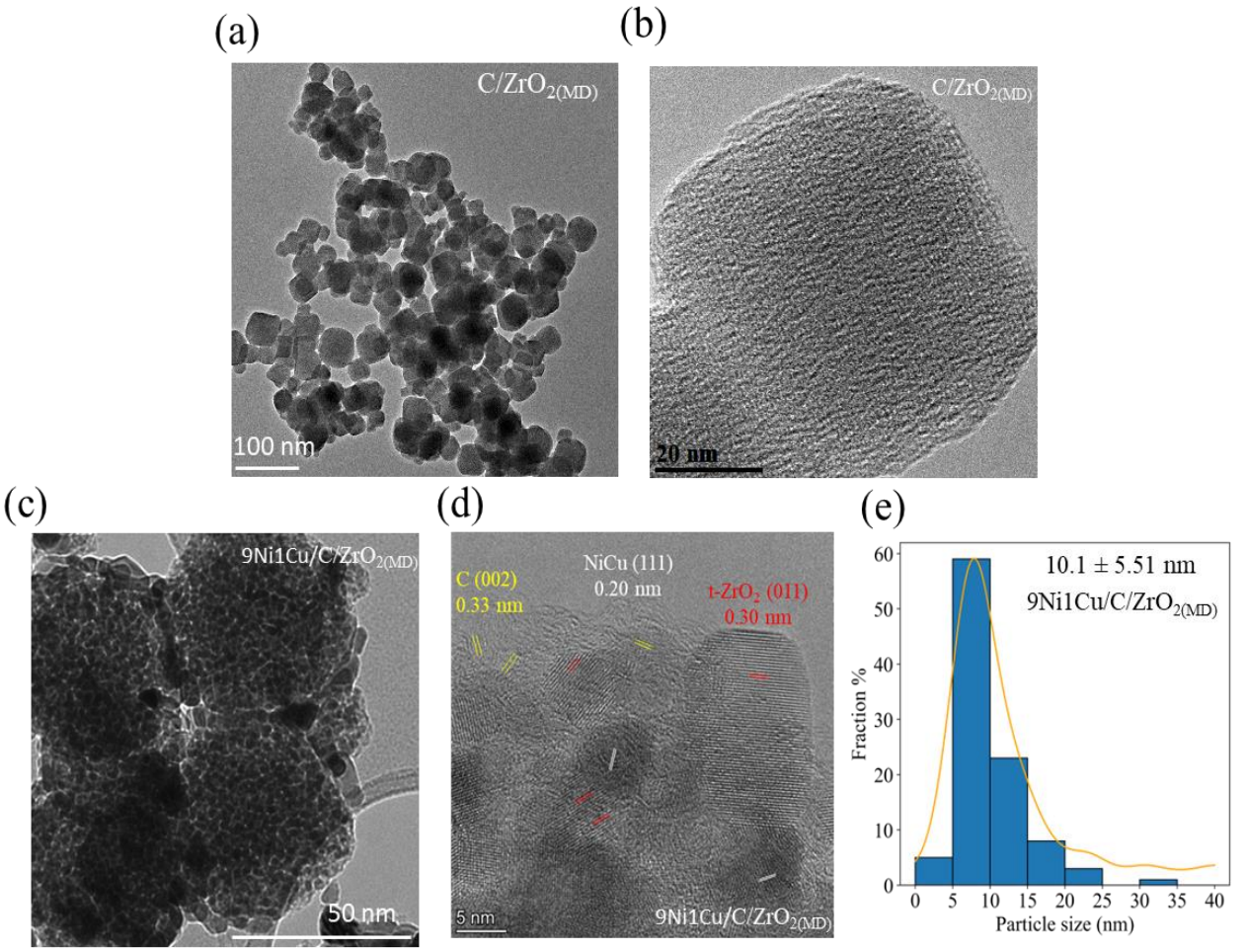

Fig. 3 (a) TEM and (b) HRTEM images of $C/ZrO_{2(MD)}$; (c) TEM, (d) HR-TEM images, and (e) Ni/Cu particle size distribution of $9Ni1Cu/C/ZrO_{2(MD)}$.

improvement in DRM performance. The C/t-ZrO2 framework effectively constrains NiCu nanoparticles, averting their aggregation through enhanced metal dispersion. Simultaneously, it establishes pathways that facilitate the diffusion of both gaseous reactants and products within and out of the catalyst.

To further investigate the porosity of $C/ZrO_{2(MD)}$-based catalysts, N_2 adsorption/desorption isotherms at 77 K were analyzed on reduced $C/ZrO_{2(MD)}$ and $ZrO_{2(DC)}$ based catalysts by the Brunauer–Emmett–Teller (BET) method. As observed from the BET isotherms in Fig. 4a, a high adsorption capacity is with $C/ZrO_{2(MD)}$, which has a BET surface area (S_{BET}) of 973 m^2/g, consistent with the literature[58,59] while $ZrO_{2(DC)}$ only had a S_{BET} of 30 m^2/g (Table 1), indicating a bulk structure with few pores. The loading of metals reduced the surface area. For $C/ZrO_{2(MD)}$ based catalysts, after loading with 10Ni or 9Ni1Cu, S_{BET} decreased to 183 and 120 m^2/g, respectively. It was found that 9Ni1Cu reduced the surface area more than 10Ni. From TEM images, edges of $C/ZrO_{2(MD)}$ were unclear to be observed in the $10Ni/C/ZrO_{2(MD)}$ catalyst, indicating possible Ni aggregation on the $C/ZrO_{2(MD)}$ surface (Fig. S2), while majority of 9Ni1Cu filled the pores thus reduced the surface area slightly more. In addition, mesopores dominate in $C/ZrO_{2(MD)}$ and $C/ZrO_{2(MD)}$-based catalysts and $C/ZrO_{2(MD)}$ has a total pore volume (V_P) of 0.492 cm^3/g, about 10 times that of $ZrO_{2(DC)}$ (Table 1). For $C/ZrO_{2(MD)}$-based catalysts, after loading with 10Ni or 9Ni1Cu nanoparticles, the pores of $C/ZrO_{2(MD)}$ with diameters > 10 nm disappeared, leaving pores with diameters < 10 nm (Fig. 4b). A lower pore volume of small pores (centered at ~2.7 nm) was measured in $9Ni1Cu/C/ZrO_{2(MD)}$ than $10Ni/C/ZrO_{2(MD)}$, suggesting that NiCu alloy nanoparticles are more likely confined in those smaller pores and better dispersed on $C/ZrO_{2(MD)}$ compared to single metallic Ni nanoparticles. In contrast, a very small pore volume of $9Ni1Cu/ZrO_{2(DC)}$ was detected, indicating a non-porous structure.

The results of CO_2 adsorption/desorption isotherms at 298 K are presented in Fig. 4c. $C/ZrO_{2(MD)}$ demonstrated a high CO_2 uptake, evidence of its advanced CO_2 adsorption ability. This ability has also been proved in previous research in CO_2 capture and separation applications.[60,61] On the other hand, $ZrO_{2(DC)}$ was not effective in CO_2 adsorption. On $C/ZrO_{2(MD)}$-based catalysts, after loading with 10Ni or 9Ni1Cu, the CO_2 uptake decreased, likely due to the reduced pore volume. Furthermore, $9Ni1Cu/C/ZrO_{2(MD)}$ had a higher CO_2 uptake than $10Ni/C/ZrO_{2(MD)}$, suggesting that Cu benefited CO_2 adsorption in Ni-Cu alloy.[62] Previous theoretical studies also suggested that Cu has a lower CO_2 adsorption energy barrier

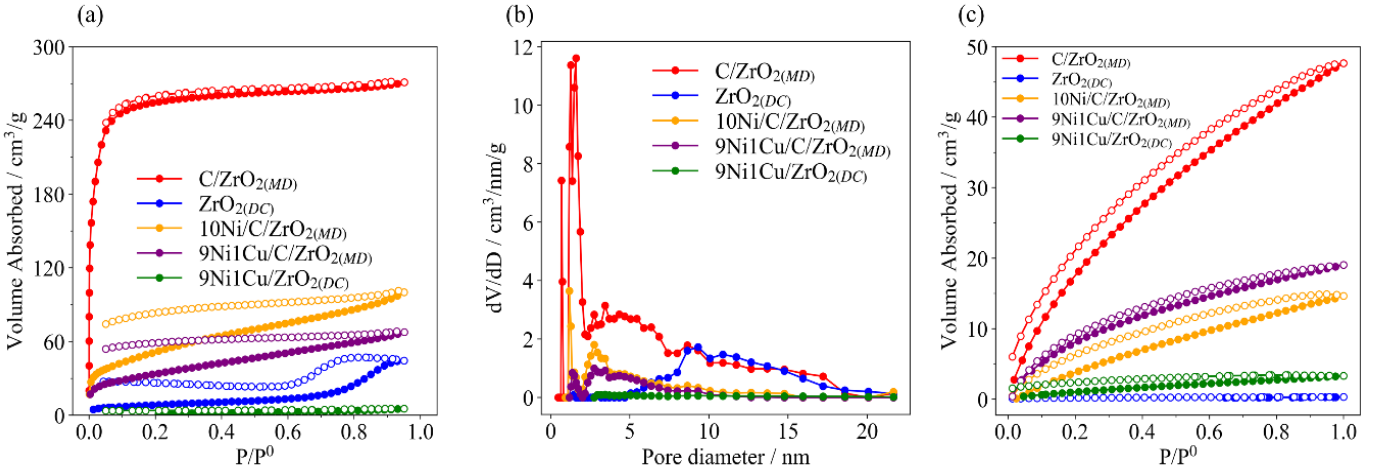

Fig. 4 (a) Nitrogen adsorption/desorption isotherms; (b) Pore diameter distribution of the catalysts; (c) CO_2 adsorption/desorption isotherms.

and activation energy barrier than Ni,[63,64] while the enhanced adsorption of CO_2 can potentially decrease the carbon formation by promoting reverse Boudouard reaction.

Table 1. Physicochemical properties.

Sample	S_{BET} (m^2/g)	V_p (cm^3/g)
$C/ZrO_{2(MD)}$	973	0.492
$ZrO_{2(DC)}$	30.0	0.055
$10Ni/C/ZrO_{2(MD)}$	183	0.08
$9Ni1Cu/C/ZrO_{2(MD)}$	120	0.06
$9Ni1Cu/ZrO_{2(DC)}$	6.00	0.005

Chemical states of Ni ad Cu species were analyzed by XPS. Fig. 5a and Fig. S4a show the deconvolution of the high-resolution XPS spectra of Ni 2p. The Ni 2p 3/2 peak at ~852 eV is attributed to metallic Ni^0, the one at ~855 eV is associated with satellite peak of Ni^{2+}, and the one at ~861 eV is related to satellite peak of Ni^0. The Ni 2p 1/2 peak at ~881 eV is attributed to satellite peak of Ni^{2+}, and the one at ~873 eV is associated with Ni^{2+}.[22,65] In Fig. 5b and Fig. S4b, two peaks at ~932 eV and ~952 eV corresponds to Cu^0 or Cu^{1+} 2p 3/2 and 2p 1/2, while no obvious peaks associated with Cu^{2+} were detected, indicating its reduction.[19] The relative surface concentrations of Ni and Cu on catalysts were also calculated (Table S1). It was found that the Ni surface concentration on $ZrO_{2(MD)}$-based catalysts was much lower than $ZrO_{2(DC)}$-based catalyst, indicating that majority of Ni was indeed confined in the $ZrO_{2(MD)}$ nanostructure while Ni-Cu was mainly located on the surface of $ZrO_{2(DC)}$.

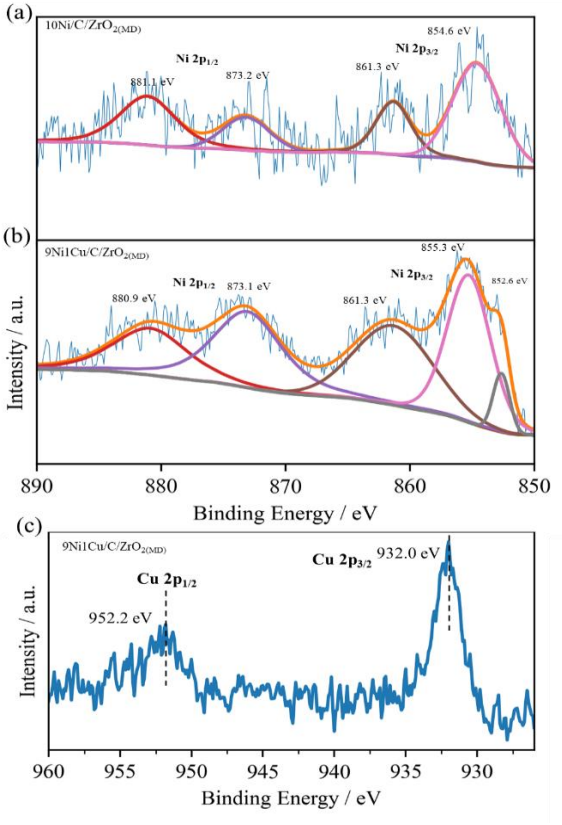

Fig. 5 Ni 2p of (a) $10Ni/C/ZrO_{2(MD)}$, (b) $9Ni1Cu/C/ZrO_{2(MD)}$, and (c) Cu 2p of $9Ni1Cu/C/ZrO_{2(MD)}$ catalysts.

3.2. Evaluation of DRM activities

The performance was measured on 4 catalysts, $9Ni1Cu/C/ZrO_{2(MD)}$, $10Ni/C/ZrO_{2(MD)}$, $9Ni1Cu/ZrO_{2(DC)}$, and $10Ni/ZrO_{2(DC)}$ at four different GHSV from 78 to 624 L g_{cat}^{-1} h^{-1} and at temperatures from 500 to 700 °C.

To investigate the behavior of mass-transfer resistance, we first conducted DRM experiments for different catalysts at four flow rates, and the average 1st-h DRM results are presented in Fig. 6. With an increasing GHSV, the residence time of reactant on the catalysts as well as the reactant conversion and product yield were reduced for all catalysts. However, it is obvious that the $C/ZrO_{2(MD)}$-based catalysts experienced much less mass-transfer resistance compared with $ZrO_{2(DC)}$-based catalysts, evidenced by a less degree of DRM performance drops when GHSV increased from 78 to 624 L g_{cat}^{-1} h^{-1} (Table S2). As generally accepted, DRM occurs via dual sites such that CO_2 reduction active sites are on metal oxides while CH_4 dissociation sites are on metals.[1] This performance drop difference can indicate nanoconfinement of NiCu NPs for CH_4 dissociation in $C/ZrO_{2(MD)}$-based catalysts, while on $ZrO_{2(DC)}$-based catalyst, NiCu NPs were on the outer surface thus suffered more performance loss as gas flow rate

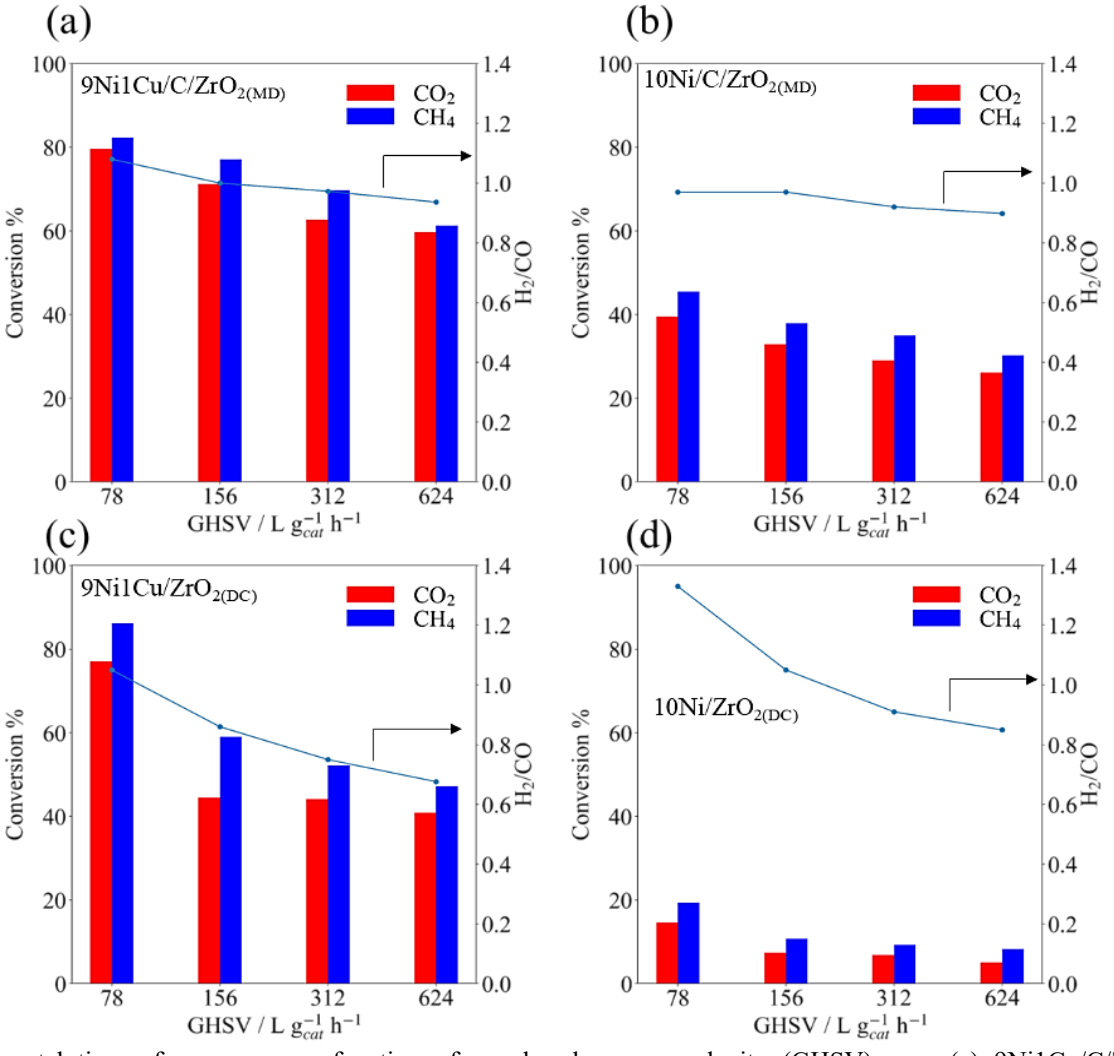

Fig. 6 DRM catalytic performance as a function of gas hourly space velocity (GHSV) over (a) 9Ni1Cu/C/$ZrO_{2(MD)}$, (b) 10Ni/C/$ZrO_{2(MD)}$, (c) 9Ni1Cu/$ZrO_{2(DC)}$, (d) 10Ni/$ZrO_{2(DC)}$ at reaction temperature of 700 °C.

increases. Similarly, Fujitsuka *et al.* reported that by increasing the GHSV 10 times, a zeolite-encapsulated Ni catalyst suffered a much smaller CH_4 conversion compared to zeolite-supported Ni catalyst, which is the due to the highly thermal stable encapsulation structure that leads to small Ni particles for efficient DRM performance.[66] In addition, with Cu addition, both C/$ZrO_{2(MD)}$ and $ZrO_{2(DC)}$ based catalyst showed a lower drop of CO_2 conversion value, showing the promotional role of Cu in CO_2 reduction. Omran *et al.* discovered that Cu doping in Ni favored the CO_2 hydrogenation process thus promoting the CO_2 dissociation,[67] while Song *et al.* claimed that Cu metal can be more readily oxidized by CO_2 compared to Ni metal thus served as the CO_2 dissociation sites in the Ni-Cu alloy structure.[19] Song *et al.* documented that the inclusion of copper additionally acted as the site for CO_2 dissociation, leading to the generation of more active oxygen species crucial for carbon gasification.[19] Therefore, both the MOF structure and Cu addition mitigated the performance loss with increasing gas flow rate.

The influence of reaction temperatures on DRM process was also investigated. The C/$ZrO_{2(MD)}$-based catalysts were evaluated from 500 to 700 °C and the average 1st-h DRM results were presented in Fig. S5. For all catalysts, CO_2 and CH_4 conversions increased gradually versus temperature, as it is widely acceptable that DRM is an endothermic process. In addition, the largest slope for each conversion curve is observed from 550 to 600 °C, which suggested that the threshold efficient temperature is within this range so that DRM dominates over side reactions after this temperature.[22] The dependence between DRM performance and Ni/Cu weight ratio of C/$ZrO_{2(MD)}$-based catalysts were further investigated, and the average 1st-h DRM results are presented in Fig. 7. The highest DRM performance was achieved on 9Ni1Cu/C/$ZrO_{2(MD)}$, with CO_2 and CH_4 conversion at 80% and 82%, respectively, and H_2/CO molar ratio at 1.08. The catalysts with nominal Ni/Cu weight ratio of 9/1 and 7/3 both achieved higher DRM performance than monometallic Ni, while a further increase of the Cu content gradually lowered the DRM performance. It is possible that excessive Cu addition to Ni may form individual Cu nanoparticles that have a higher CH_4 activation barrier than Ni nanoparticles, thus making DRM process less efficient.[18] The monometallic Cu catalyst had only 10% CO_2 conversion and 12% CH_4 conversion, further proving that Cu is less active than Ni.

Besides MOF confined NiCu catalysts in this study, previous literature also reported similar influence of Ni/Cu ratio on DRM performance on catalysts supported on metal oxides, for example, Mg/Al oxides and SiO_2.[18,19] In those works, the optimal catalysts were identified to have a small Cu concentration, similar to our work on C/$ZrO_{2(MD)}$-based catalysts.

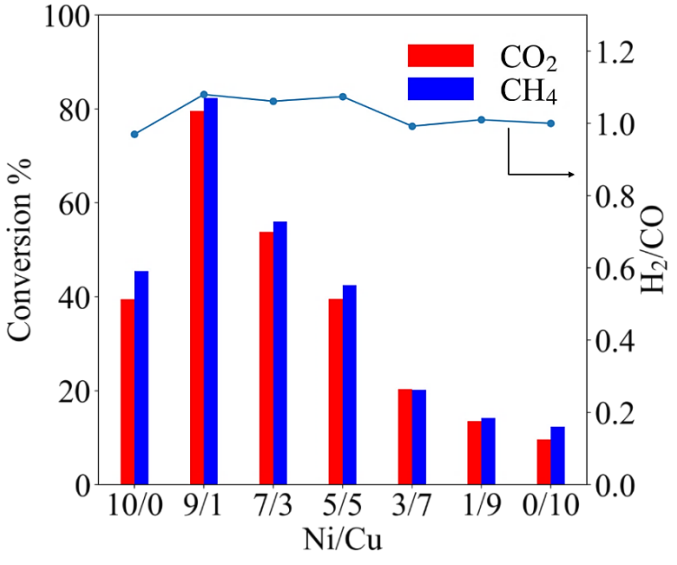

Fig. 7 DRM catalytic performance with varied Ni/Cu weight ratio of C/$ZrO_{2(MD)}$-based catalyst at reaction temperature of 700 °C, GHSV = 78 $Lg_{cat}^{-1}h^{-1}$.

3.3 Evaluation of DRM stabilities

Long-term stability tests were conducted for the C/$ZrO_{2(MD)}$ and $ZrO_{2(DC)}$ based catalysts at 700 °C and 78 L g_{cat}^{-1} h^{-1}, and the results are presented in Fig. 8 and Fig. S6. In the 100 h DRM test, 9Ni1Cu/C/$ZrO_{2(MD)}$demonstrated the best performance, with 76% CO_2 conversion and 77% CH_4 conversion and a H_2/CO molar ratio of 1.07, averaging throughout the duration of 100 h. Without Cu addition, 10Ni/C/$ZrO_{2(MD)}$ showed much less CO_2 and CH_4 conversion, averaged at 45% and 46%, respectively. The C/$ZrO_{2(MD)}$-based catalysts also demonstrated much better activity than $ZrO_{2(DC)}$-based catalysts. During the 24 h DRM testing, 9Ni1Cu/$ZrO_{2(DC)}$ showed an average 61% CO_2 and 66% CH_4 conversion, and 0.96 H_2/CO ratio. The activity of 10Ni/$ZrO_{2(DC)}$ was much worse, only 17% CO_2 conversion and 19% CH_4 conversion, and 1.21 H_2/CO ratio.

Additionally, the C/$ZrO_{2(MD)}$-based catalysts also received better stability than $ZrO_{2(DC)}$-based catalysts. It is observed on 9Ni1Cu/C/$ZrO_{2(MD)}$ that the initial CO_2 and CH_4 conversion was even increased for the first 20 h. For the rest 80 h, CO_2 and CH_4 conversion on 9Ni1Cu/C/$ZrO_{2(MD)}$ had only a slight decrease. By comparing the performance with the leading DRM catalysts in the literature (Table 2), the 9Ni1Cu/C/$ZrO_{2(MD)}$ stands among the leading performers regarding average conversions of CO_2 and CH_4 in a long-term (*i.e.*, 100 h) experiment. In contrast, the initial performance of 9Ni1Cu/$ZrO_{2(DC)}$ is notable, attributed to the accessibility of metals on the outer surface but dropped quickly over the course of 24 h, a much faster deactivation rate than 9Ni1Cu/C/$ZrO_{2(MD)}$. For both 10Ni/C/$ZrO_{2(MD)}$ and 10Ni/$ZrO_{2(DC)}$, the CO_2 and CH_4 conversion dropped quickly in the first few hours and leveled off for the rest of the testing period.

3.4 Mechanistic understanding of structure-performance relationships

Because 9Ni1Cu/C/$ZrO_{2(MD)}$ has demonstrated the best DRM performance among all the prepared catalysts, here we further unveil the possible relationships between structural advantages and DRM performance including the unique MOF-derived structure and bimetallic composition. The analysis of spent catalysts was carried out to unveil correlations between the catalyst properties with DRM

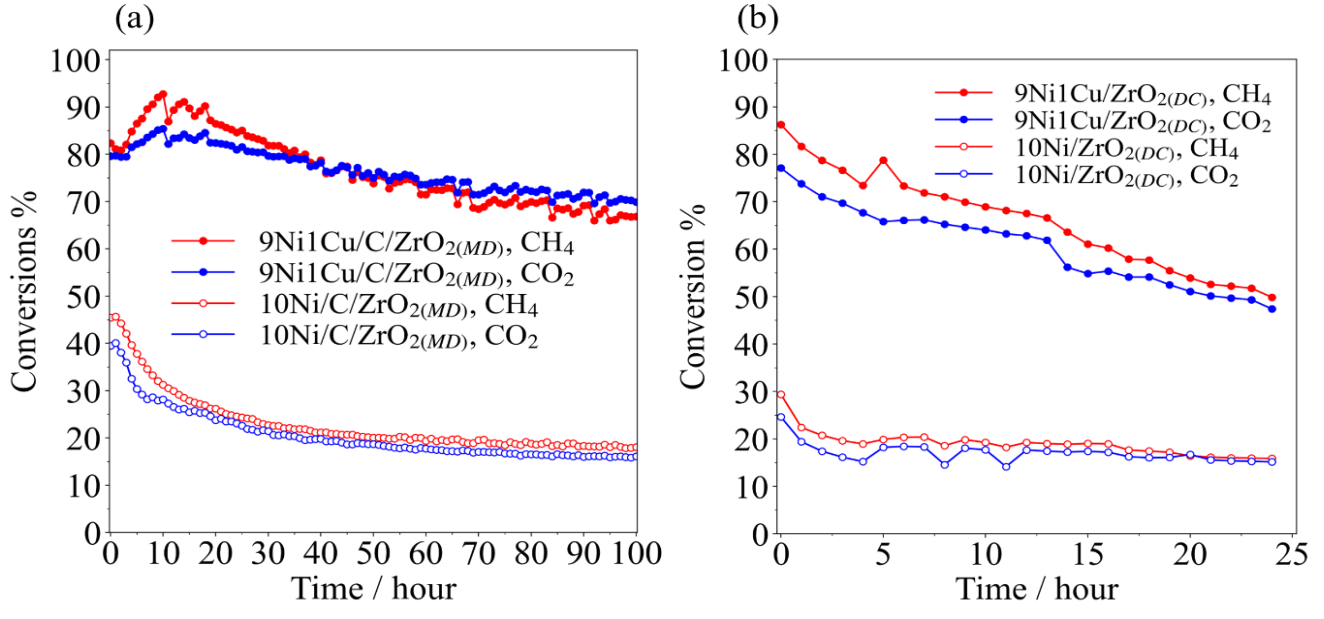

Fig. 8 Long-term CO_2 and CH_4 conversion of (a) C/$ZrO_{2(MD)}$-based catalysts and (b) $ZrO_{2(DC)}$-based catalysts at reaction temperature of 700 °C, GHSV = 78 $Lg_{cat}^{-1}h^{-1}$.

Table 2. Comparison of DRM performance in this work with the literature.

Catalyst	Temp (°C)	Flow rate (sccm)	CO_2:CH_4: balance gas	Conversion (%)		H_2/CO	Stability	Ref.
				CO_2	CH_4			
9Ni1Cu/C/$ZrO_{2(MD)}$	700	8	1:1:8	76	77	1.07	100 h	This work
3NiAS	750	15	1:1	64.2	53.7	N/A	100 h	[21]
NiCo@C/Al_2O_3	700	200	1:1:18	76-57	43	0.9	8 h	[31]
Ni-BEA	700	50	2:2:1	76	78	0.9	12 h	[68]
5ZrO_2-Ni/Al_2O_3	700	60	1:1	~85	77	0.8	50 h	[23]
Ni-Cu/Mg(Al)O	600	50	1:1:2	60	47	0.68	25 h	[19]
NiCo@CMOF-74	700	-	1:1	65	57	0.82	10 h	[69]
75Ni25Co/$MgAl_2O_4$	600	-	1:1:1.5	13	9	0.5	3 h	[70]
Ni-Co/Al_2O_3-S	800	50	1:1:8	N/A	76	1	60 h	[71]
Ni-Sn/CeO_2-Al_2O_3	700	25	1:1:6	90-70	70	0.87	20 h	[72]
Ru-Ni/$MgAl_2O_4$	800	400	1:1	75	96	0.61	6 h	[73]
NiFe/MgO	760	50	1:1	70	63	0.78	100 h	[74]

performance.[1] Fig. 9 shows TEM images of spent 9Ni1Cu/C/$ZrO_{2(MD)}$ and 10Ni/C/$ZrO_{2(MD)}$ after 100 h DRM experiments and spent 9Ni1Cu/$ZrO_{2(DC)}$ and 10Ni/$ZrO_{2(DC)}$ after 24 h DRM, after their long-term stability test. Particles with diameter more than 60 nm were observed on spent 10Ni/C/$ZrO_{2(MD)}$, 9Ni1Cu/$ZrO_{2(DC)}$, 10Ni/$ZrO_{2(DC)}$, and large amounts of filamentous carbon were clearly observed on $ZrO_{2(DC)}$-based catalysts but were absent on 9Ni1Cu/C/$ZrO_{2(MD)}$. Therefore, it is inferred that Cu doping played a more vital role in preventing metal sintering. Similarly, Chatla *et al*. reported that Cu addition with a Cu to Ni weight ratio of 1 to 8 benefited Ni dispersion on Al_2O_3.[76] Their DFT calculations indicated that adding Cu elevated the activation energy barrier for complete dehydrogenation of CH_4 to C while considerably decreasing the energy barrier for oxidation of deposited carbon. Song *et al*. also suggested that Cu alloying on hydrotalcite-derived Ni/Mg(Al)O catalyst inhibited CH_4 decomposition and facilitated CO_2 dissociation, yielding more active oxygen species crucial for carbon to be gasified, thus enhancing the catalytic stability.[19] Therefore, the Cu doping indispensably contributed to the most stable performance of 9Ni1Cu/C/$ZrO_{2(MD)}$ catalyst in this work.

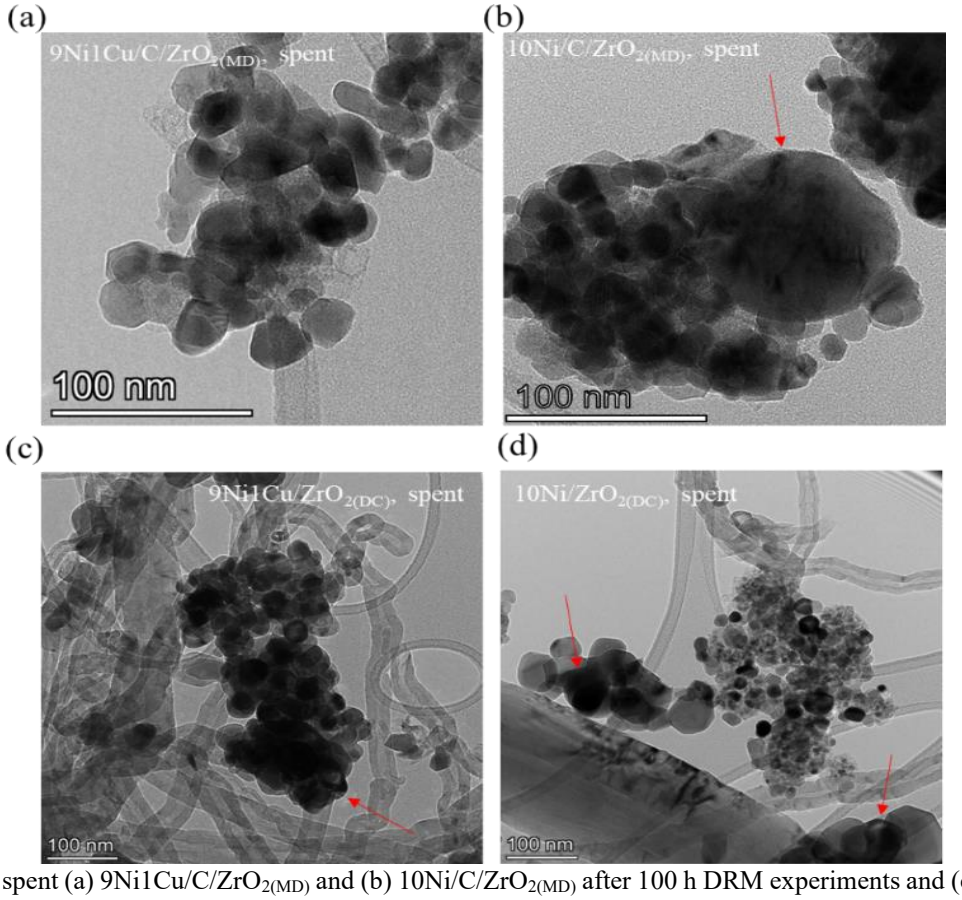

Fig. 9 TEM images of spent (a) 9Ni1Cu/C/$ZrO_{2(MD)}$ and (b) 10Ni/C/$ZrO_{2(MD)}$ after 100 h DRM experiments and (c) 9Ni1Cu/$ZrO_{2(DC)}$ and (d) 10Ni/$ZrO_{2(DC)}$ after 24 h DRM experiments (red arrow: metal aggregations).

Besides Cu, other early transition metal (ETM) can potentially promote Ni-based catalysts' performance and compete with noble metals for industrial application due to their cost-effectiveness.[15,77] To investigate whether MOF-derived framework can be applied for other ETM metals besides Cu, bimetallic catalysts alloying Ni with a second metal (M_2 = Fe, Co, Mo) at the same weight ratio (*i.e.*, 9/1) were prepared and confined in the C/$ZrO_{2(MD)}$ support; their DRM catalytic activities were measured and presented in Fig. S7. Compared with monometallic Ni catalyst, bimetallic Ni/Cu and Ni/Fe promoted the DRM activity, while Ni/Co and Ni/Mo had negative effects. Bimetallic Ni/Cu was the highest performing catalyst.

Thermogravimetric analysis (TGA) and XPS analysis were further performed to compare the as-synthesized and spent catalysts (Fig. S8 and Fig. 10). A weight loss of 61.5% was observed on the as-synthesized 9Ni1Cu incorporated MOF (*i.e.* as-prepared 9Ni1Cu/C/$ZrO_{2(MD)}$ before reaction), which was due to the decomposition of MOF structure to carbon/ZrO_2 (C/$ZrO_{2(MD)}$). As for the spent catalysts, 9Ni1Cu/C/$ZrO_{2(MD)}$ and 9Ni1Cu/$ZrO_{2(DC)}$ suffered a 21.0% and 27.0% weight loss, respectively. The weight loss of spent 9Ni1Cu/C/$ZrO_{2(MD)}$ can happen due to the oxidation of two sources of carbon. One carbon comes from the decomposition of MOF, and the other carbon comes from the carbon produced during the DRM process. For 9Ni1Cu/$ZrO_{2(DC)}$, the weight loss is solely due to the oxidation of carbon produced from DRM process. The higher weight loss of 9Ni1Cu/$ZrO_{2(DC)}$ indicated higher produced carbon from DRM, in agreement with the TEM results and its worse DRM stability. Additionally, the XPS characterization was conducted on spent 9Ni1Cu/C/$ZrO_{2(MD)}$ and 9Ni1Cu/$ZrO_{2(DC)}$ to probe the chemical states of Ni and Cu and showed in Fig. 10. All Ni^0 concentration on spent catalysts became higher than it on fresh catalysts, which can be due to the reducing environment of DRM. Both Ni and Cu peaks signals were also weak on spent 9Ni1Cu/$ZrO_{2(DC)}$, probably due to coverage of deposited carbon. More importantly, Ni^0 fraction of the total Ni element concentration is still higher on spent 9Ni1Cu/C/$ZrO_{2(MD)}$ catalyst than spent 9Ni1Cu/$ZrO_{2(DC)}$ catalyst (Table S3), which can be due to the MOF-derived C/t-ZrO_2 provided a better metal-support interaction and metal dispersion thus restricting the metal aggregation. The higher concentration of Ni^0 on spent catalysts indicated the reducing environment of DRM.

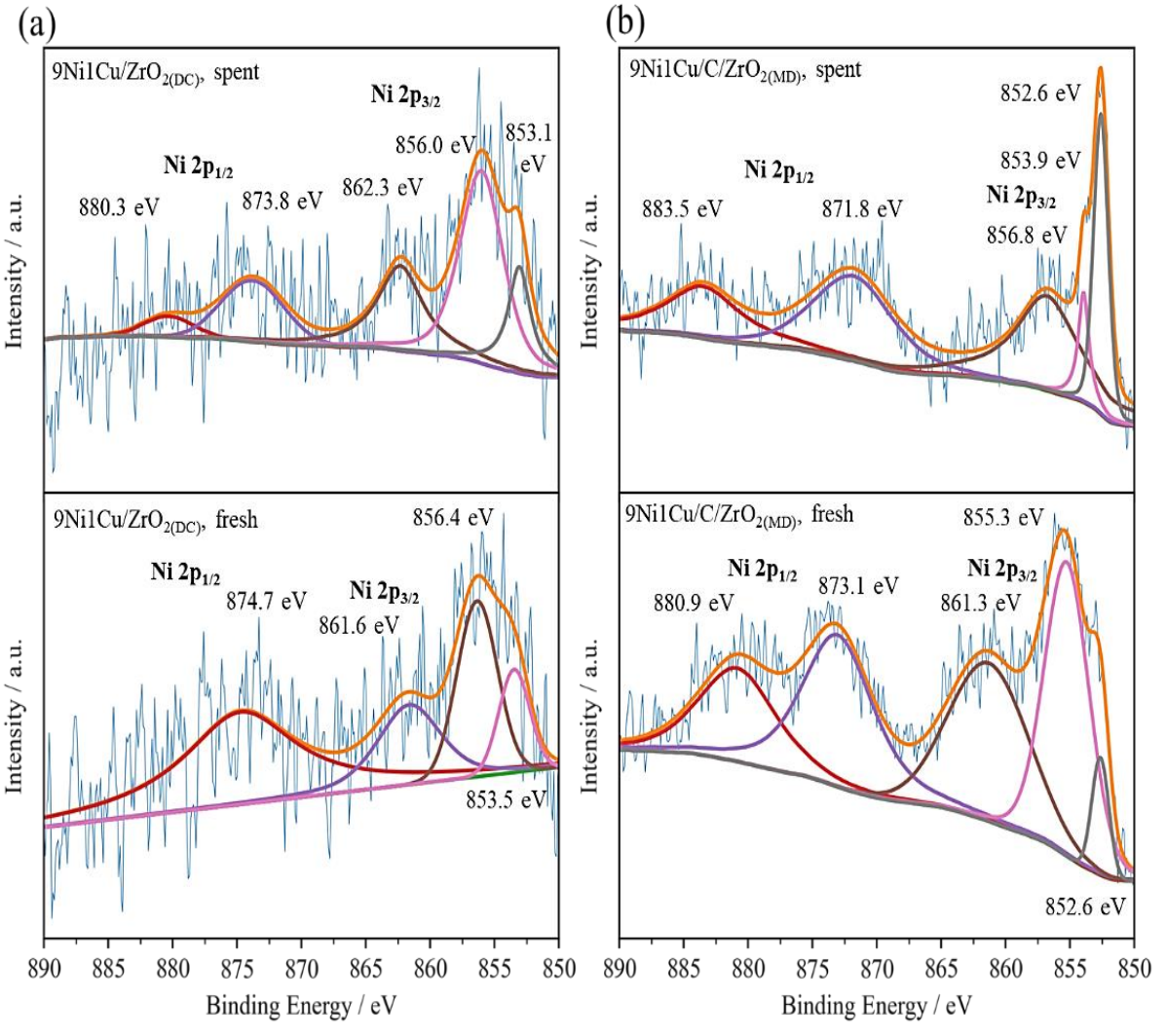

Fig. 10 Ni 2p XPS spectra of fresh and spent catalysts for (a) 9Ni1Cu/C/$ZrO_{2(MD)}$ after 100 h and (b) 9Ni1Cu/$ZrO_{2(DC)}$ after 24 h DRM experiments.

4. Conclusion

In this study, an efficient and stable DRM catalyst (9Ni1Cu/C/$ZrO_{2(MD)}$) was developed by applying MOF templates to confine NiCu nanoparticles in a porous and large surface area ZrO_2 support. The C/t-ZrO_2 framework played a vital role in enhancing metal-support interacton, facilitating reactant gas diffusion, and hindering the aggregation of NiCu nanoparticles and carbon deposition. The formation of Ni-Cu alloy resulted in a smaller nanoparticle alloy size than monometallic Ni, and Cu addition benefited CO_2 adsorption/conveersion and NiO reducibility to Ni. These benefits largely promoted the DRM performance of 9Ni1Cu/C/$ZrO_{2(MD)}$ and made it much higher and more stable than directly-calcination prepared ZrO_2 supported 9Ni1Cu catalysts. The obtained average 100 h CO_2 and CH_4 conversions and H_2/CO ratio on 9Ni1Cu/C/$ZrO_{2(MD)}$ were among the top state-of-the-art catalysts. Our catalyst design provides a facile and efficient catalyst suitable for various catalytic reactions.

Acknowledgements

This work was supported by U.S. National Science Foundation (Grant No. 1924466). The use of Materials Characterization Facility (MCF) at Texas A&M University is acknowledged. Los Alamos National Laboratory is operated by Triad National Security, LLC, for the National Nuclear Security Administration of the US Department of Energy under contract no. 89233218CNA000001. The opinions and perspectives expressed by the author do not necessarily represent or reflect the US Government or any of its agencies. The US Government, its agencies, and their employees make no expressed or implied warranties and assume no legal liability or responsibility for the accuracy, completeness, or usefulness of any disclosed information, apparatus, product, or process. Additionally, it is not implied that the use of such information would not infringe on privately owned rights.

Conflict of Interest

There is no conflict of interest.

Supporting Information

Applicable.

References

[1] A. Abdulrasheed, A. A. Jalil, Y. Gambo, M. Ibrahim, H. U. Hambali, M. Y. Shahul Hamid, A review on catalyst development for dry reforming of methane to syngas: recent advances, *Renewable and Sustainable Energy Reviews*, 2019, **108**, 175-193, doi: 10.1016/j.rser.2019.03.054.

[2] X. Cai, Y. H. Hu, Advances in catalytic conversion of methane and carbon dioxide to highly valuable products, *Energy Science & Engineering*, 2019, **7**, 4-29, doi: 10.1002/ese3.278.

[3] W.-J. Jang, J.-O. Shim, H.-M. Kim, S.-Y. Yoo, H.-S. Roh, A review on dry reforming of methane in aspect of catalytic properties, *Catalysis Today*, 2019, **324**, 15-26, doi: 10.1016/j.cattod.2018.07.032.

[4] Z. Xie, B. Yan, S. Kattel, J. H. Lee, S. Yao, Q. Wu, N. Rui, E. Gomez, Z. Liu, W. Xu, L. Zhang, J. G. Chen, Dry reforming of methane over CeO_2-supported Pt-Co catalysts with enhanced activity, *Applied Catalysis B: Environmental*, 2018, **236**, 280-293, doi: 10.1016/j.apcatb.2018.05.035.

[5] N. Abdel Karim Aramouni, J. G. Touma, B. Abu Tarboush, J. Zeaiter, M. N. Ahmad, Catalyst design for dry reforming of methane: analysis review, *Renewable and Sustainable Energy Reviews*, 2018, **82**, 2570-2585, doi: 10.1016/j.rser.2017.09.076.

[6] D. Pakhare, J. Spivey, A review of dry (CO_2) reforming of methane over noble metal catalysts, *Chemical Society Reviews*, 2014, **43**, 7813-7837, doi: 10.1039/c3cs60395d.

[7] F. Pan, X. Xiang, W. Deng, H. Zhao, X. Feng, Y. Li, A novel photo-thermochemical approach for enhanced carbon dioxide reforming of methane, *ChemCatChem*, 2018, **10**, 940-945, doi: 10.1002/cctc.201701565.

[8] J. Deng, K. Bu, Y. Shen, X. Zhang, J. Zhang, K. Faungnawakij, D. Zhang, Cooperatively enhanced coking resistance via boron nitride coating over Ni-based catalysts for dry reforming of methane, *Applied Catalysis B: Environmental*, 2022, **302**, 120859, doi: 10.1016/j.apcatb.2021.120859.

[9] A. L.-A. Marinho, F. S. Toniolo, F. B. Noronha, F. Epron, D. Duprez, N. Bion, Highly active and stable Ni dispersed on mesoporous CeO_2-Al_2O_3 catalysts for production of syngas by dry reforming of methane, *Applied Catalysis B: Environmental*, 2021, **281**, 119459, doi: 10.1016/j.apcatb.2020.119459.

[10] Y. H. Hu, E. Ruckenstein, Comment on "Dry reforming of methane by stable Ni–Mo nanocatalysts on single-crystalline MgO", *Science*, 2020, **368**, eabb5459, doi: 10.1126/science.abb5459.

[11] O. Muraza, A. Galadima, A review on coke management during dry reforming of methane, *International Journal of Energy Research*, 2015, **39**, 1196-1216, doi: 10.1002/er.3295.

[12] Z. Hou, J. Gao, J. Guo, D. Liang, H. Lou, X. Zheng, Deactivation of Ni catalysts during methane autothermal reforming with CO_2 and O_2 in a fluidized-bed reactor, *Journal of Catalysis*, 2007, **250**, 331-341, doi: 10.1016/j.jcat.2007.06.023.

[13] E. C. Lovell, A. Fuller, J. Scott, R. Amal, Enhancing Ni-SiO 2 catalysts for the carbon dioxide reforming of methane: reduction-oxidation-reduction pre-treatment, *Applied Catalysis B: Environmental*, 2016, **199**, 155-165, doi: 10.1016/j.apcatb.2016.05.080.

[14] Z. Bian, S. Das, M. H. Wai, P. Hongmanorom, S. Kawi, A review on bimetallic nickel-based catalysts for CO_2 reforming of methane, *Chemphyschem*, 2017, **18**, 3117-3134, doi: 10.1002/cphc.201700529.

[15] I. V. Yentekakis, P. Panagiotopoulou, G. Artemakis, A review of recent efforts to promote dry reforming of methane (DRM) to syngas production via bimetallic catalyst formulations, *Applied Catalysis B: Environmental*, 2021, **296**, 120210, doi: 10.1016/j.apcatb.2021.120210.

[16] J. Guo, C. Xie, K. Lee, N. Guo, J. T. Miller, M. J. Janik, C. Song, Improving the carbon resistance of Ni-based steam reforming catalyst by alloying with Rh: A computational study coupled with reforming experiments and EXAFS.

[17] D. Li, Y. Nakagawa, K. Tomishige, Methane reforming to synthesis gas over Ni catalysts modified with noble metals, *Applied Catalysis A: General*, 2011, **408**, 1-24, doi: 10.1016/j.apcata.2011.09.018.

[18] K. Han, S. Wang, Q. Liu, F. Wang, Optimizing the Ni/Cu ratio in Ni–Cu nanoparticle catalysts for methane dry reforming, *ACS Applied Nano Materials*, 2021, **4**, 5340-5348, doi: 10.1021/acsanm.1c00673.

[19] K. Song, M. Lu, S. Xu, C. Chen, Y. Zhan, D. Li, C. Au, L. Jiang, K. Tomishige, Effect of alloy composition on catalytic performance and coke-resistance property of Ni-Cu/Mg(Al)O catalysts for dry reforming of methane, *Applied Catalysis B: Environmental*, 2018, **239**, 324-333, doi: 10.1016/j.apcatb.2018.08.023.
[20] Y. Yang, Y.-A. Lin, X. Yan, F. Chen, Q. Shen, L. Zhang, N. Yan, Cooperative atom motion in Ni–Cu nanoparticles during the structural evolution and the implication in the high-temperature catalyst design, *ACS Applied Energy Materials*, 2019, **2**, 8894-8902, doi: 10.1021/acsaem.9b01923.
[21] L.-Y. Shi, Y.-X. Li, D.-M. Xue, P. Tan, Y. Jiang, X.-Q. Liu, L.-B. Sun, Fabrication of highly dispersed nickel in nanoconfined spaces of as-made SBA-15 for dry reforming of methane with carbon dioxide, *Chemical Engineering Journal*, 2020, **390**, 124491, doi: 10.1016/j.cej.2020.124491.
[22] S. Xu, T. J. A. Slater, H. Huang, Y. Zhou, Y. Jiao, C. M. A. Parlett, S. Guan, S. Chansai, S. Xu, X. Wang, C. Hardacre, X. Fan, Developing silicalite-1 encapsulated Ni nanoparticles as sintering-/ coking-resistant catalysts for dry reforming of methane, *Chemical Engineering Journal*, 2022, **446**, 137439, doi: 10.1016/j.cej.2022.137439.
[23] B. Jin, S. Li, Y. Liu, X. Liang, Engineering metal-oxide interface by depositing ZrO_2 overcoating on Ni/Al_2O_3 for dry reforming of methane, *Chemical Engineering Journal*, 2022, **436**, 135195, doi: 10.1016/j.cej.2022.135195.
[24] H. Qu, H. Yang, L. Han, S. He, J. Liu, R. Hu, H. Su, Y. Su, Sandwich-structured nickel/kaolinite catalyst with boosted stability for dry reforming of methane with carbon dioxide, *Chemical Engineering Journal*, 2023, **453**, 139694, doi: 10.1016/j.cej.2022.139694.
[25] L. Jiao, Y. Wang, H.-L. Jiang, Q. Xu, Metal-organic frameworks as platforms for catalytic applications, *Advanced Materials*, 2018, **30**, e1703663, doi: 10.1002/adma.201703663.
[26] S. Dang, Q.-L. Zhu, Q. Xu, Nanomaterials derived from metal-organic frameworks, *Nature Reviews Materials*, 2018, **3**, 17075, doi: 10.1038/natrevmats.2017.75.
[27] X. Li, X. Yang, H. Xue, H. Pang, Q. Xu, Metal–organic frameworks as a platform for clean energy applications, *EnergyChem*, 2020, **2**, 100027, doi: 10.1016/j.enchem.2020.100027.
[28] W. Xia, A. Mahmood, R. Zou, Q. Xu, Metal–organic frameworks and their derived nanostructures for electrochemical energy storage and conversion, *Energy & Environmental Science*, 2015, **8**, 1837-1866, doi: 10.1039/c5ee00762c.
[29] A. Indra, T. Song, U. Paik, Metal organic framework derived materials: progress and prospects for the energy conversion and storage, *Advanced Materials*, 2018, **30**, 1705146, doi: 10.1002/adma.201705146.
[30] Z. Li, L. Mo, Y. Kathiraser, S. Kawi, Yolk–satellite–shell structured Ni–Yolk@Ni@SiO_2 nanocomposite: superb catalyst toward methane CO_2 reforming reaction, *ACS Catalysis*, 2014, **4**, 1526-1536, doi: 10.1021/cs401027p.
[31] T. Y. Liang, D. Senthil Raja, K. C. Chin, C. L. Huang, S. A. Sethupathi, L. K. Leong, D. H. Tsai, S. Y. Lu, Bimetallic metal-organic framework-derived hybrid nanostructures as high-performance catalysts for methane dry reforming, *ACS Applied Materials & Interfaces*, 2020, **12**, 15183-15193, doi: 10.1021/acsami.0c00086.
[32] A. Dhakshinamoorthy, A. Santiago-Portillo, A. M. Asiri, H. Garcia, Engineering UiO-66 metal organic framework for heterogeneous catalysis, *ChemCatChem*, 2019, **11**, 899-923, doi: 10.1002/cctc.201801452.
[33] F. Bi, X. Zhang, S. Xiang, Y. Wang, Effect of Pd loading on ZrO_2 support resulting from pyrolysis of UiO-66: application to CO oxidation, *Journal of Colloid Interface Science*, 2020, **573**, 11-20, doi: 10.1016/j.jcis.2020.03.120.
[34] T. Wang, F. Li, H. An, W. Xue, Y. Wang, Enhanced catalytic activity over palladium supported on ZrO_2@C with NaOH-assisted reduction for decomposition of formic acid, *RSC Advances*, 2019, **9**, 3359-3366, doi: 10.1039/c8ra10198a.
[35] D. Wang, P. Littlewood, T. J. Marks, P. C. Stair, E. Weitz, Coking can enhance product yields in the dry reforming of methane, *ACS Catalysis*, 2022, **12**, 8352-8362, doi: 10.1021/acscatal.2c02045.
[36] Z. Du, F. Pan, X. Yang, L. Fang, Y. Gang, S. Fang, T. Li, Y. H. Hu, Y. Li, Efficient photothermochemical dry reforming of methane over Ni supported on ZrO_2 with CeO_2 incorporation, *Catalysis Today*, 2023, **409**, 31-41, doi: 10.1016/j.cattod.2022.05.014.
[37] R. Shen, T.-H. Yan, R. Ma, E. Joseph, Y. Quan, H.-C. Zhou, Q. Wang, Flammability and thermal kinetic analysis of UiO-66-based PMMA polymer composites, *Polymers*, 2021, **13**, 4113, doi: 10.3390/polym13234113.
[38] X. Feng, Z. Du, E. Sarnello, W. Deng, C. R. Petru, L. Fang, T. Li, Y. Li, Syngas production at a near-unity H_2/CO ratio from photo-thermo-chemical dry reforming of methane on a Pt decorated Al_2O_3–CeO_2 catalyst, *Journal of Materials Chemistry A*, 2022, **10**, 7896-7910, doi: 10.1039/d1ta10088b.
[39] Z. Du, F. Pan, E. Sarnello, X. Feng, Y. Gang, T. Li, Y. Li, Probing the origin of photocatalytic effects in photothermochemical dry reforming of methane on a Pt/CeO_2 catalyst, *The Journal of Physical Chemistry C*, 2021, **125**, 18684-18692, doi: 10.1021/acs.jpcc.1c04152.
[40] M. C. Campa, G. Ferraris, D. Gazzoli, I. Pettiti, D. Pietrogiacomi, Rhodium supported on tetragonal or monoclinic ZrO_2 as catalyst for the partial oxidation of methane, *Applied Catalysis B: Environmental*, 2013, **142-143**, 423-431, doi: 10.1016/j.apcatb.2013.05.046.
[41] X. Zhang, M. Zhang, J. Zhang, Q. Zhang, N. Tsubaki, Y. Tan, Y. Han, Methane decomposition and carbon deposition over Ni/ZrO_2 catalysts: comparison of amorphous, tetragonal, and monoclinic zirconia phase, *International Journal of Hydrogen Energy*, 2019, **44**, 17887-17899, doi: 10.1016/j.ijhydene.2019.05.174.
[42] G. Bonura, C. Cannilla, F. Frusteri, Ceria–gadolinia supported NiCu catalyst: a suitable system for dry reforming of biogas to feed a solid oxide fuel cell (SOFC), *Applied Catalysis B: Environmental*, 2012, **121-122**, 135-147, doi: 10.1016/j.apcatb.2012.03.028.
[43] T. Liang, Y. Wang, M. Chen, Z. Yang, S. Liu, Z. Zhou, X. Li, Steam reforming of phenol-ethanol to produce hydrogen over bimetallic Ni Cu catalysts supported on sepiolite, *International Journal of Hydrogen Energy*, 2017, **42**, 28233-28246, doi: 10.1016/j.ijhydene.2017.09.134.
[44] Q. Guo, Z. Guo, J. Shi, L. Sang, B. Gao, Q. Chen, X. Wang, Z. Liu, Fabrication of nickel and nickel carbide thin films by pulsed chemical vapor deposition, *MRS Communications*, 2018, **8**, 88-94, doi: 10.1557/mrc.2018.21.
[45] J. Kang, R. Han, J. Wang, L. Yang, G. Fan, F. Li, *In situ* synthesis of nickel carbide-promoted nickel/carbon nanofibers nanocomposite catalysts for catalytic applications, *Chemical*

Engineering Journal, 2015, **275**, 36-44, doi: 10.1016/j.cej.2015.04.024.
[46] B. Tang, W.-C. Song, E.-C. Yang, X.-J. Zhao, MOF-derived Ni-based nanocomposites as robust catalysts for chemoselective hydrogenation of functionalized nitro compounds, *RSC Advances*, 2017, **7**, 1531-1539, doi: 10.1039/C6RA26699A.
[47] J. Deng, P. Ren, D. Deng, X. Bao, Enhanced electron penetration through an ultrathin graphene layer for highly efficient catalysis of the hydrogen evolution reaction, *Angewandte Chemie International Edition*, 2015, **54**, 2100-2104, doi: 10.1002/anie.201409524.
[48] S. M. M. Nataj, S. M. Alavi, G. Mazloom, Modeling and optimization of methane dry reforming over Ni–Cu/Al_2O_3 catalyst using Box–Behnken design, *Journal of Energy Chemistry*, 2018, **27**, 1475-1488, doi: 10.1016/j.jechem.2017.10.002.
[49] N. Bayat, M. Rezaei, F. Meshkani, Methane dissociation to COx-free hydrogen and carbon nanofiber over Ni-Cu/Al_2O_3 catalysts, *Fuel*, 2017, **195**, 88-96, doi: 10.1016/j.fuel.2017.01.039.
[50] J. Ashok, M. Subrahmanyam, A. Venugopal, Hydrotalcite structure derived Ni–Cu–Al catalysts for the production of H_2 by CH_4 decomposition, *International Journal of Hydrogen Energy*, 2008, **33**, 2704-2713, doi: 10.1016/j.ijhydene.2008.03.028.
[51] D. Li, M. Koike, J. Chen, Y. Nakagawa, K. Tomishige, Preparation of Ni–Cu/Mg/Al catalysts from hydrotalcite-like compounds for hydrogen production by steam reforming of biomass tar, *International Journal of Hydrogen Energy*, 2014, **39**, 10959-10970, doi: 10.1016/j.ijhydene.2014.05.062.
[52] A. Chatla, M. M. Ghouri, O. W. El Hassan, N. Mohamed, A. V. Prakash, N. O. Elbashir, An experimental and first principles DFT investigation on the effect of Cu addition to Ni/Al_2O_3 catalyst for the dry reforming of methane, *Applied Catalysis A: General*, 2020, **602**, 117699, doi: 10.1016/j.apcata.2020.117699.
[53] Z.-W. Zhao, X. Zhou, Y.-N. Liu, C.-C. Shen, C.-Z. Yuan, Y.-F. Jiang, S.-J. Zhao, L.-B. Ma, T.-Y. Cheang, A.-W. Xu, Ultrasmall Ni nanoparticles embedded in Zr-based MOFs provide high selectivity for CO_2 hydrogenation to methane at low temperatures, *Catalysis Science & Technology*, 2018, **8**, 3160-3165, doi: 10.1039/c8cy00468d.
[54] M. Mihet, O. Grad, G. Blanita, T. Radu, M. D. Lazar, Effective encapsulation of Ni nanoparticles in metal-organic frameworks and their application for CO_2 methanation, *International Journal of Hydrogen Energy*, 2019, **44**, 13383-13396, doi: 10.1016/j.ijhydene.2019.03.259.
[55] Y. Gang, E. Sarnello, J. Pellessier, S. Fang, M. Suarez, F. Pan, Z. Du, P. Zhang, L. Fang, Y. Liu, T. Li, H.-C. Zhou, Y. H. Hu, Y. Li, One-step chemical vapor deposition synthesis of hierarchical Ni and N Co-doped carbon nanosheet/nanotube hybrids for efficient electrochemical CO_2 reduction at commercially viable current densities, *ACS Catalysis*, 2021, **11**, 10333-10344, doi: 10.1021/acscatal.1c01864.
[56] C. Ghosh, D. Ramachandran, G. Balakrishnan, P. Kuppusami, E. Mohandas, HRTEM investigation of phase stability in alumina–zirconia multilayer thin films, *Bulletin of Materials Science*, 2015, **38**, 401-407, doi: 10.1007/s12034-014-0838-z.
[57] J. Hou, Y. Sun, Z. Li, B. Zhang, S. Cao, Y. Wu, Z. Gao, L. Sun, Electrical behavior and electron transfer modulation of nickel–copper nanoalloys confined in nickel–copper nitrides nanowires array encapsulated in nitrogen-doped carbon framework as robust bifunctional electrocatalyst for overall water splitting, *Advanced Functional Materials*, 2018, **28**, 1803278, doi: 10.1002/adfm.201803278.
[58] K. Užarević, T. C. Wang, S.-Y. Moon, A. M. Fidelli, J. T. Hupp, O. K. Farha, T. Friščić, Mechanochemical and solvent-free assembly of zirconium-based metal–organic frameworks, *Chemical Communications*, 2016, **52**, 2133-2136, doi: 10.1039/C5CC08972G.
[59] C. L. Luu, T. T. Van Nguyen, T. Nguyen, T. C. Hoang, Synthesis, characterization and adsorption ability of UiO-66-NH_2, *Advances in Natural Sciences: Nanoscience and Nanotechnology*, 2015, **6**, 025004, doi: 10.1088/2043-6262/6/2/025004.
[60] Y. Cao, H. Zhang, F. Song, T. Huang, J. Ji, Q. Zhong, W. Chu, Q. Xu, UiO-66-NH_2/GO composite: synthesis, characterization and CO_2 adsorption performance, *Materials*, 2018, **11**, 589, doi: 10.3390/ma11040589.
[61] Q. Yang, A. D. Wiersum, H. Jobic, V. Guillerm, C. Serre, P. L. Llewellyn, G. Maurin, Understanding the thermodynamic and kinetic behavior of the CO_2/CH_4 gas mixture within the porous zirconium terephthalate UiO-66(Zr): a joint experimental and modeling approach, *The Journal of Physical Chemistry C*, 2011, **115**, 13768-13774, doi: 10.1021/jp202633t.
[62] Y. Liu, D. Liu, Study of bimetallic Cu–Ni/γ-Al_2O_3 catalysts for carbon dioxide hydrogenation, *International Journal of Hydrogen Energy*, 1999, **24**, 351-354, doi: 10.1016/s0360-3199(98)00038-x.
[63] Y. Shi, K. Han, F. Wang, Ni–Cu alloy nanoparticles confined by physical encapsulation with SiO_2 and chemical metal–support interaction with CeO_2 for methane dry reforming, *Inorganic Chemistry*, 2022, **61**, 15619-15628, doi: 10.1021/acs.inorgchem.2c02466.
[64] K. Homlamai, T. Maihom, S. Choomwattana, M. Sawangphruk, J. Limtrakul, Single-atoms supported (Fe, Co, Ni, Cu) on graphitic carbon nitride for CO_2 adsorption and hydrogenation to formic acid: first-principles insights, *Applied Surface Science*, 2020, **499**, 143928, doi: 10.1016/j.apsusc.2019.143928.
[65] F. Goodarzi, L. Kang, F. R. Wang, F. Joensen, S. Kegnæs, J. Mielby, Methanation of carbon dioxide over zeolite-encapsulated nickel nanoparticles, *ChemCatChem*, 2018, **10**, 1566-1570, doi: 10.1002/cctc.201701946.
[66] H. Fujitsuka, T. Kobayashi, T. Tago, Development of Silicalite-1-encapsulated Ni nanoparticle catalyst from amorphous silica-coated Ni for dry reforming of methane: achieving coke formation suppression and high thermal stability, *Journal of CO_2 Utilization*, 2021, **53**, 101707, doi: 10.1016/j.jcou.2021.101707.
[67] A. Omran, S. H. Yoon, M. Khan, M. Ghouri, A. Chatla, N. Elbashir, Mechanistic insights for dry reforming of methane on Cu/Ni bimetallic catalysts: DFT-assisted microkinetic analysis for coke resistance, *Catalysts*, 2020, **10**, 1043, doi: 10.3390/catal10091043.
[68] S. Kweon, Y. W. Kim, C.-H. Shin, M. B. Park, H.-K. Min, Nickel silicate beta zeolite prepared by interzeolite transformation: a highly active and stable catalyst for dry reforming of methane, *Chemical Engineering Journal*, 2022, **431**, 133364, doi: 10.1016/j.cej.2021.133364.
[69] I. S. Khan, A. Ramirez, G. Shterk, L. Garzón-Tovar, J. Gascon, Bimetallic metal-organic framework mediated synthesis of Ni-co catalysts for the dry reforming of methane, *Catalysts*, 2020, **10**, 592, doi: 10.3390/catal10050592.

[70] R. Kumari, S. Sengupta, Catalytic CO_2 reforming of CH_4 over $MgAl_2O_4$ supported Ni-Co catalysts for the syngas production, *International Journal of Hydrogen Energy*, 2020, **45**, 22775-22787, doi: 10.1016/j.ijhydene.2020.06.150.
[71] Z. Wu, B. Yang, S. Miao, W. Liu, J. Xie, S. Lee, M. J. Pellin, D. Xiao, D. Su, D. Ma, Lattice Strained Ni-Co alloy as a High-Performance Catalyst for Catalytic Dry Reforming of Methane, *ACS Catalysis*, 2019, **9**, 2693-2700, doi: 10.1021/acscatal.8b02821.
[72] T. Stroud, T. J. Smith, E. Le Saché, J. L. Santos, M. A. Centeno, H. Arellano-Garcia, J. A. Odriozola, T. R. Reina, Chemical CO_2 recycling via dry and bi reforming of methane using Ni-Sn/Al_2O_3 and Ni-Sn/CeO_2-Al_2O_3 catalysts, *Applied Catalysis B: Environmental*, 2018, **224**, 125-135, doi: 10.1016/j.apcatb.2017.10.047.
[73] I. Wysocka, J. Hupka, A. Rogala, Catalytic activity of nickel and ruthenium–nickel catalysts supported on SiO_2, ZrO_2, Al_2O_3, and $MgAl_2O_4$ in a dry reforming process, *Catalysts*, 2019, **9**, 540, doi: 10.3390/catal9060540.
[74] T. Zhang, Z. Liu, Y.-A. Zhu, Z. Liu, Z. Sui, K. Zhu, X. Zhou, Dry reforming of methane on Ni-Fe-MgO catalysts: influence of Fe on carbon-resistant property and kinetics, *Applied Catalysis B: Environmental*, 2020, **264**, 118497, doi: 10.1016/j.apcatb.2019.118497.
[75] X. Zhang, J. Qiao, C. Liu, F. Wang, Y. Jiang, P. Cui, Q. Wang, Z. Wang, L. Wu, J. Liu, A MOF-derived ZrO_2/C nanocomposite for efficient electromagnetic wave absorption, *Inorganic Chemistry Frontiers*, 2020, **7**, 385-393, doi: 10.1039/C9QI01259A.
[76] X. Gao, Z. Ge, G. Zhu, Z. Wang, J. Ashok, S. Kawi, Anti-coking and anti-sintering Ni/Al_2O_3 catalysts in the dry reforming of methane: recent progress and prospects, *Catalysts*, 2021, **11**, 1003, doi: 10.3390/catal11081003.
[77] H. Liu, T. D. Dao, L. Liu, X. Meng, T. Nagao, J. Ye, Light assisted CO_2 reduction with methane over group VIII metals: universality of metal localized surface plasmon resonance in reactant activation, *Applied Catalysis B: Environmental*, 2017, **209**, 183-189, doi: 10.1016/j.apcatb.2017.02.080.

